Implications of the effective axial-vector coupling of gluon on top-quark charge asymmetry at the LHC

Emidio Gabrielli,[1,*] Antonio Racioppi,[1,†] and Martti Raidal[1,‡]

[1] *NICPB, Ravala 10, 10143 Tallinn, Estonia*

We study different top quark charge asymmetries and the variation of $t\bar{t}$ total cross section induced by the effective axial-vector coupling of gluon in the LHC experiments. We show that rapidity cut-dependent asymmetries are more sensitive to the new physics than the independent ones. We also study the dependence of the asymmetries and variations of total $t\bar{t}$ cross sections on the invariant mass of $t\bar{t}$ system and show that it would be necessary to measure those quantities as functions of m_{tt} at the LHC. In the context of considered new physics scenario, 7 TeV LHC has enough sensitivity either to confirm the Tevatron top asymmetry anomaly or to rule it out. In the latter case the LHC is able to put stringent constraint on the new physics scale Λ in this framework.

I. INTRODUCTION

The more than 3σ excess in top quark charge asymmetry observed both by the CDF [1] and, more recently, by the D0 [2] experiments at the Tevatron compared to the standard model (SM) predictions [3–6] has triggered numerous theoretical and experimental studies of top quark production at hadron colliders. An intriguing property of the measured asymmetry is that it increases with the $t\bar{t}$ invariant mass m_{tt}. At the same time the measured $t\bar{t}$ production cross section is consistent, within experimental errors, with the SM predictions [7–11] both at Tevatron [12, 13] and at the LHC [14, 15]. Motivated by those results, the SM predictions for $t\bar{t}$ charge asymmetry have been revised in [16, 17] showing moderate 20% increase due to QED and electroweak (EW) corrections.

Numerous new physics (NP) scenarios (see [18] for a recent review) have been proposed to explain the observed anomaly that predict the existence of new particles whose contributions induce the asymmetry. Those scenarios can be directly tested at the LHC experiments by looking for new particle interactions. In the light of LHC results several popular explanations to the $t\bar{t}$ charge asymmetry such as the axigluons [19–21], Z' [22] or W' [23] are stringently constrained.

However, effective field theory offers also model-independent tests of the top quark charge asymmetry. Particularly interesting among those is the one due to the effective axial-vector coupling of the gluon [24]. This scenario does predict the correct sign and the correct m_{tt} dependence of the Tevatron anomaly and does not necessarily require new light resonances. Therefore tests of this scenario require particularly precise measurement of the top quark charge asymmetry dependence on m_{tt}.

As shown in [24], the characteristic new physics scale Λ, associated to a universal effective axial-vector coupling of the gluon, should lie in a narrow range $\Lambda \simeq [1 - 1.3]$ TeV, in order to correctly reproduce the Tevatron anomaly on top-quark charge asymmetry. The lower bound on $\Lambda > 1$ TeV comes mainly by requiring conservative constraints on the total cross section of top-quark pair production, which is enhanced by the presence of an effective axial-vector coupling. Therefore, the characteristic new physics scale associated to this scenario is within the discovery potential of LHC. We will discuss in more details this issue in section IV.

Although the LHC is pp collider with symmetric initial state, the $t\bar{t}$ charge asymmetry can be also defined and studied at the LHC in $q\bar{q}$ collisions using anti-quarks from the sea [3, 4]. Because the sea quark parton distributions differ from the valence ones, top and anti-top quark are preferably produced in different rapidities. Therefore, as shown in [16], studying top quark charges asymmetries at large rapidities and large invariant masses will enhance the asymmetries both in the SM as well as in NP scenarios. At present the ATLAS [25] and CMS [26] experiments have published only their measurements of rapidity cut-independent top quark charge asymmetries. Their results are consistent with the SM predictions. No rapidity nor invariant mass dependent observables for top quark charge asymmetry have been studied at the LHC, since the top-quark statistics is not yet large enough.

The aim of this work is to study rapidity cut and invariant mass dependent top quark charge asymmetries at the LHC in the scenario of effective axial-vector coupling of the gluon. We show that the rapidity and invariant mass dependent asymmetries are much more appropriate for testing this type of NP scenarios than the cut-independent ones used by the ATLAS and CMS experiments so far. As a result, the Tevatron observation of large $t\bar{t}$ charge asymmetry, that in $p\bar{p}$ collisions is equivalent to the $t\bar{t}$ forward-backward asymmetry A^t_{FB}, can be either confirmed or ruled out already in the 7 TeV LHC with 10 fb^{-1} data. In the latter case the LHC is able to put stringent constraint on the NP scale Λ in this framework.

The paper is organized as follows. In section II we review the theoretical framework of the effective field theory that generates the axial-vector coupling of the gluon. In section III we study the effects of this scenario on

*emidio.gabrielli@cern.ch
†antonio.racioppi@kbfi.ee
‡martti.raidal@cern.ch

the $t\bar{t}$ total cross section at the LHC. In section IV we define different rapidity cut-dependent and independent charge asymmetries and present the results of our numerical studies. We conclude in section V.

II. THEORETICAL FRAMEWORK

The most general effective Lagrangian for a generic quark-gluon interaction, containing the lowest dimensional operators, and compatible with gauge-, CP-, and Lorentz-invariance, is [24]

$$\begin{aligned}\mathcal{L} &= -ig_S\Big\{\bar{Q}T^a\left[\gamma^\mu\left(1+g_V(q^2,M)+\gamma_5 g_A(q^2,M)\right)G^a_\mu\right.\\ &+ \left. g_P(q^2,M)q^\mu\gamma_5 G^a_\mu + g_M(q^2,M)\sigma^{\mu\nu}G^a_{\mu\nu}\right]Q\Big\}, \qquad (1)\end{aligned}$$

where g_S is the strong coupling constant, G^a_μ and $G^a_{\mu\nu}$ are the gluon field and corresponding field strength respectively, T^a are the color matrices, M is some energy scale, q^2 is the invariant momentum-squared carried by the gluon, and Q denotes a generic quark field. Sum over the color index a is understood.

At the moment we do not make any assumption on the origin of the form factors $g_{A,P}(q^2,M)$ associated to the quark Q. In the case of the SM, these form factors are induced at 1-loop by the exchange of W,Z bosons. In this case the scale M is connected to the EW scale, being related to the W,Z (masses) exchanged in the loop. However, from now on we will assume that the dominant contribution to the $g_{A,P}(q^2,M)$ arises from a NP which has a characteristic scale above the EW scale. In this case the scale M should be identified with the NP scale. The form factors $g_{A,P}$ depend also on quark masses that can be neglected for $m_Q^2 \ll M^2$. Finally, the last term in Eq. (1) is the contribution of the chromomagnetic dipole operator (with $g_M(q^2,M)$ the corresponding form factor), that may affect the total cross section [27, 28] but does not significantly contribute to the asymmetry A^t_{FB} [29], and we shall not include it in our analysis.

Model independently, the QCD gauge invariance implies a Ward identity (WI) $2m_Q g_A(q^2,M) = q^2 g_P(q^2,M)$, thus

$$\lim_{q^2\to 0} g_{A,V}(q^2,M) = 0\,, \qquad (2)$$

since no $1/q^2$ singularities are present in g_P. Notice that the Ward Identity in Eq.(2) is exact and free from any anomaly contribution, since the vector-axial coupling is an effective vertex and the fundamental theory (QCD) is anomaly free. As observed in [24], Eq. (2) does not pose any additional constraint on the form factors $g_{A,V}$, which could have different magnitudes at arbitrary q^2. Therefore, gauge-invariance does not prevent us to have $g_V \ll g_A$ as long as $q^2 \neq 0$. We stress here once again that the QCD gauge invariance is not broken and gluon remains massless because g_A and g_V are induced via the form factors in Eq. (1) that are subject to the condition in Eq. (2).

As stressed above, the $g_{V,A}$ exist also in the SM, where they are induced by EW radiative corrections, but are numerically too small to have significant impact on the observables we consider. However, if the origin of large A^t_{FB} observed at Tevatron is due to NP that has $(V \pm A)$ currents as in the SM, large g_V and g_A can be generated. In [24] we found that this scenario is phenomenologically unacceptable because g_V is strongly constrained by the total $q\bar{q} \to t\bar{t}$ cross section. Indeed, being $q\bar{q} \to t\bar{t}$ the dominant $t\bar{t}$ production mechanism at Tevatron, its cross section depends quadratically on g_A but only linearly on g_V. In particular, the magnitude of g_A, necessary to explain the Tevatron A^t_{FB} anomaly, is not compatible with the condition $g_A \sim g_V$, since g_V is strongly constrained by the measurements on the $p\bar{p} \to t\bar{t}$ cross section, which are in good agreement with SM predictions. However, notice that the dominant contribution to the $t\bar{t}$ production at LHC is given by the $gg \to t\bar{t}$ process, which depends quadratically on g_V. Therefore, the $t\bar{t}$ production cross section at LHC turns out to be less sensitive to g_V than at Tevatron.

Following the same approach as in [24], from now on, we will neglect the contribution of the vectorial form factor $g_V(q^2,M)$ in Eq. (1), and consider only NP scenarios that generate g_A with the hierarchy $g_V \ll g_A$. In the limit of $q^2 \ll M^2$, it is useful to parametrize the axial-vector form factor as

$$g_A(q^2,M) = \frac{q^2}{\Lambda^2}F(q^2,\Lambda)\,, \qquad (3)$$

where we absorb the NP coupling α_{NP} and loop factor into the NP scale, $\Lambda^2 = M^2/(4\pi\alpha_{NP})$. Because of the breaking of conformal invariance, induced by renormalization, we expect [30] $F(q^2,\Lambda)$ to contain also logarithm terms $\log(q^2/\Lambda^2)$. This could give a large log enhancement in the case of $|q^2| \ll \Lambda^2$. In general, the form factor $F(q^2,\Lambda)$ could also develop an imaginary part for $q^2 > 0$. In perturbation theory, this is related to the absorptive part of the loop diagram generating g_A, when $|q^2|$ is above the threshold of some specific particles pair production.

In [24], an origin of the anomalous large g_A has been suggested. Assuming that there is a perturbative NP above the EW scale, model independently the effective operators [31]

$$O^{1,8}_{AV} = \frac{1}{\Lambda^2}[\bar{Q}T_{1,8}\gamma^\mu\gamma_5 Q][\bar{Q}T_{1,8}\gamma^\mu Q]\,, \qquad (4)$$

$$O^{1,8}_{PS} = \frac{1}{\Lambda^2}[\bar{Q}T_{1,8}\gamma_5 Q][\bar{Q}T_{1,8}Q], \qquad (5)$$

generate g_A via 1-loop diagrams depicted in Fig. 1. Here $T_1 = 1$ and $T_8 = T^a$, thus both isoscalar and octet operators contribute. Notice that: (i) no g_V is induced due to the CP odd property of the operators in Eqs.(4),(5) and to QCD parity conservation; (ii) the 1-loop induced g_A can be enhanced by large $\log(q^2/\Lambda^2)$, although in this

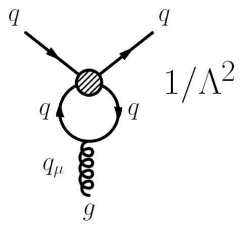

FIG. 1: Feynman diagram in the effective low energy theory that generates the effective axial-vector coupling of gluon, where Λ is the scale related to the contact four-quarks operator.

case the large logs need to be resummed via the renormalization group methods; (*iii*) the operators $O^{1,8}_{AV}$, $O^{1,8}_{PS}$ do not induce FC processes; however, there could be different quark flavors in the loop in Fig. 1 (extending the operator basis to $Q \to Q'$, $V \leftrightarrow A$, $P \leftrightarrow S$ is straightforward); (*iv*) the operators $O^{1,8}_{AV}$, $O^{1,8}_{PS}$ do not interfere with the corresponding QCD induced 4-quark processes. The latter point has very important implications for our scenario – the stringent LHC constraints [32, 33] on 4-quark contact interactions do not apply at all. Indeed, those constraints come from the interference between QCD and NP diagrams, and constrain the models that explain A^t_{FB} with the similar interference very stringently. We stress that our scenario is free from those constraints and NP at 1-2 TeV can induce large g_A as explained above.

However, the presence in the effective Lagrangian of the operators in Eqs. (4),(5) without the counterparts of dimension-6 operators $O^{1,8}_{VV}$ and $O^{1,8}_{AA}$ (or analogously $O^{1,8}_{SS}$ and $O^{1,8}_{PP}$) suppressed by a scale of the same order of Λ, suggests more a scenario in which the above contact interactions are a manifestation of quark compositeness, rather than the exchange of a heavy (perturbative) resonances among fundamental quark fields. We do not elaborate on such a high scale NP model here.

Alternatively, large g_A might be generated by new strongly-coupled parity-violating dynamics related to EW symmetry breaking (EWSB) at 1-2 TeV scale. Because this NP is entirely non-perturbative, generating g_A is possible [34] but we are not able to compute it. We are only able to estimate the validity range of the effective coupling parametrization in Eq. (3) that is controlled by $\hat{s}/\Lambda^2_{eff}$, where Λ^2_{eff} is expected to be related to Λ as $\Lambda_{eff} \sim \Lambda/\sqrt{\alpha_S}$. For $\Lambda \sim 1(1.3)$ TeV, as required by the A^t_{FB} anomaly, the related scale Λ_{eff} is 3.5 (4.6) TeV. At this scale a plethora of new resonances should occur at the LHC allowing to test this scenario. Notice that, in the region of large invariant masses $\hat{s} \gg \Lambda^2_{eff}$, the low-energy ansatz $g_A \sim q^2/\Lambda^2$ is not valid anymore and the q^2 dependence of g_A should be determined by fitting the data. Unitarity should require that $g_A \leq 1$ at large exchanged momenta $|q^2| \gg \Lambda^2$, bounding the anomalous behavior of the total cross section with energy.

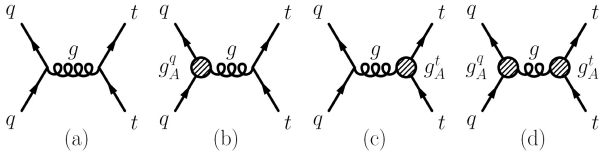

FIG. 2: Feynman diagrams (a)-(d) for the $q\bar{q} \to t\bar{t}$ process, with the contribution of the gluon effective axial-vector couplings $g^{q,t}_A$.

III. CROSS SECTIONS

Here we analyze the contribution of the axial-vector g_A anomalous coupling, as defined in Eq. (1), to the partonic cross sections for $t\bar{t}$ pair production at the LHC, related to the processes $q\bar{q} \to t\bar{t}$ and $gg \to t\bar{t}$.

A. $q\bar{q} \to t\bar{t}$ process

Let us consider the tree-level scattering

$$q(p_1)\bar{q}(p_2) \to t(p_3)\bar{t}(p_4)\,, \tag{6}$$

where p_{1-4} are the corresponding particles momenta and q stands for a light quark. The Feynman diagrams (a)-(d) relative to $q\bar{q} \to t\bar{t}$, including the axial-vector coupling, are shown in Fig. 2. According to Eq. (1), supplemented by the Ward identity in Eq. (2), the Feynman rule $\Gamma^{a\ \mu}_{A}$, corresponding to the effective axial-vector gluon couplings to quarks q is

$$\Gamma^{a\ \mu}_{A} = i g^q_A\, T^a \left(\gamma_\mu\gamma_5 - 2q_\mu \frac{m_q}{q^2}\gamma_5\right)\,, \tag{7}$$

where q_μ is the gluon momentum entering the vertex, m_q is the quark mass, and T^a the color matrix. From now on, we will omit the q^2 dependence in the g^q_A form factors, unless specified. The corresponding differential cross section in the massless light-quarks q limit (summed over all colors) is given by

$$\begin{aligned}\frac{d\sigma^{q\bar{q}}}{d\hat{t}} &= \frac{8\pi\alpha_S^2}{9\hat{s}^4}\Big[\Big(\hat{t}^2 + (\hat{s}-2m_t^2)\hat{t} + \frac{\hat{s}^2}{2} + m_t^4\Big)\times \\ &\quad \left(1+|g^q_A|^2+|g^t_A|^2+|g^q_A|^2|g^t_A|^2\right) \\ &- 2|g^t_A|^2\, m_t^2\hat{s}\left(1+|g^q_A|^2\right) \\ &+ 2\mathrm{Re}[g^q_A]\,\mathrm{Re}[g^t_A]\,\hat{s}(\hat{s}+2\hat{t}-2m_t^2)\Big]\,,\end{aligned} \tag{8}$$

where g^q_A and g^t_A are the corresponding axial-vector form factors for the light-quark q and top-quark, respectively. The Mandelstam variables $\hat{s}, \hat{t}, \hat{u}$ are defined as

$$\hat{s} = (p_1+p_2)^2, \quad \hat{t} = (p_1-p_3)^2, \quad \hat{u} = (p_1-p_4)^2\,. \tag{9}$$

The result in Eq. (8) is gauge invariant due to the corresponding Ward identity in Eq. (2). After integrating

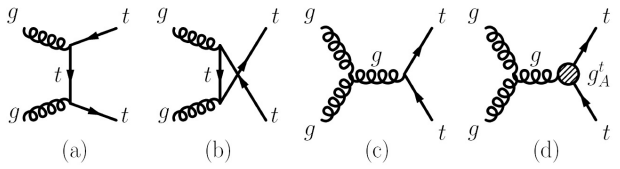

FIG. 3: Feynman diagrams (a)-(d) for the $gg \to t\bar{t}$ process, with the contribution of the gluon effective axial-vector coupling g_A^t.

Eq. (8) over the full range of $\hat{t}$, the total partonic cross section is given by [24]

$$\sigma^{q\bar{q}}(\hat{s}) = \frac{8\pi\alpha_S^2\beta_t}{27\hat{s}}\Big\{(1+2\frac{m_t^2}{\hat{s}})\left(1+|g_A^q|^2\right)+ \beta_t^2|g_A^t|^2\left(1+|g_A^q|^2\right)\Big\}, \quad (10)$$

where $\beta=\sqrt{1-\rho}$ and $\rho = 4m_t^2/\hat{s}$.

B. $gg \to t\bar{t}$ process

The Feynman diagrams relative to the tree-level process $gg \to t\bar{t}$ are shown in Fig. 3. Here, the effective axial-vector coupling of the top-quark affects only the s-channel (diagram 3(d)). Indeed, due to the Ward identity in Eq. (2), the effective axial-vector contribution vanishes in the $\hat{t}$- and $\hat{u}$-channels, diagrams 3(a) and 3(b) respectively, because the gluons attached to the axial-vector vertex are on-shell.

Finally, the differential unpolarized cross section (summed over all colors) for the $gg \to t\bar{t}$ scattering, corresponding to the Feynman diagrams in Fig. 3, is given by

$$\frac{d\sigma^{gg}}{d\hat{t}} = \frac{\pi\alpha_S^2}{64\hat{s}^2}\Big[12M_{ss}+\frac{16}{3}\left(M_{tt}+M_{uu}\right)-\frac{2}{3}M_{tu} + 6\left(M_{st}+M_{su}\right)\Big], \quad (11)$$

with

$$\begin{aligned} M_{ss} &= \frac{4}{\hat{s}^2}\left[\left(\hat{t}-m_t^2\right)\left(\hat{u}-m_t^2\right)+\left(\hat{t}\hat{u}-m_t^4\right)|g_A^t|^2\right], \\ M_{tt} &= \frac{2}{(\hat{t}-m_t^2)^2}\left[\left(\hat{t}-m_t^2\right)\left(\hat{u}-m_t^2\right)-2m_t^2\left(\hat{u}+m_t^2\right)\right], \\ M_{tu} &= \frac{4m_t^2}{(\hat{t}-m_t^2)(\hat{u}-m_t^2)}\left(\hat{s}-4m_t^2\right), \\ M_{st} &= \frac{4}{\hat{s}(\hat{t}-m_t^2)}\left[m_t^4-\hat{t}\left(\hat{s}+\hat{t}\right)\right], \end{aligned} \quad (12)$$

and $M_{uu} = M_{tt}\,\{t \leftrightarrow u\}$, $M_{su} = M_{st}\,\{t \leftrightarrow u\}$.

Although the effective axial-vector coupling affects only the M_{ss} contribution proportional to the $|g_A^t|^2$ term in Eq. (12), this contribution is actually $SU(3)_c$ gauge invariant. In order to understand that, let us decompose the amplitude for the $gg \to t\bar{t}$ process as

$$M = M^{QCD} + M_s^A, \quad (13)$$

where M^{QCD} represents the full QCD contribution to the total amplitude and M_s^A is the diagram contribution in s-channel diagram 3(d) proportional to the effective axial-vector coupling g_A, obtained by using the standard QCD Feynman rules for the 3-gluon vertex. While it does not depend on the $SU(3)_c$ gauge-fixing, due to the conservation of the effective axial-vector vertex, the M_s^A diagram alone is not manifestly $SU(3)_c$ gauge invariant under the gauge transformations on external states, namely $\epsilon_\mu^a(p_1) \to p_{1\mu}$ and $\epsilon_\mu^b(p_2) \to p_{2\mu}$, where $\epsilon_\mu^a(p_1)$ and $\epsilon_\mu^b(p_2)$ indicate the polarization vectors of initial gluons (here a, b stand for color indices). This non-invariance is due to the presence of the QCD 3-gluon vertex in the diagram 3(d). The gauge-dependent part of the M_s^A amplitude (proportional to g_A) is not canceled by the corresponding $\hat{t}$- and $\hat{u}$-channels, since the g_A contribution to these channels is vanishing due to the condition in Eq. (2) for on-shell external gluons. However, this is not a problem and it is an artifact of the effective theory. Indeed, one can always construct a full amplitude for the $gg \to q\bar{q}$ process including the g_A contribution in a manifestly gauge invariant way. Now we will prove that the result of Eq. (11), obtained by using the M amplitude in Eq. (13), can also be obtained by using a manifestly gauge invariant amplitude M_{GI}.

In order to show that, let us add to M a new contribution $\bar{M}_s^A$, which is identical to the s-channel diagram M_s^A contribution in Fig. 3(d), but with the 3-gluon vertex suitable modified. In particular, in M_s^A the Lorentz structure of the QCD 3-gluon vertex (in momentum space) $\Gamma_{\rm QCD}^{\alpha\beta\mu}$ will be replaced by a new 3-gluon vertex $\bar{\Gamma}^{\alpha\beta\mu}$ defined as

$$p_{1\alpha}\left(\Gamma_{\rm QCD}^{\alpha\beta\mu}+\bar{\Gamma}^{\alpha\beta\mu}\right) = p_{2\beta}\left(\Gamma_{\rm QCD}^{\alpha\beta\mu}+\bar{\Gamma}^{\alpha\beta\mu}\right) = 0 + \cdots, \quad (14)$$

where $\cdots$ stands for terms proportional to $p_{2\beta}$ and/or $p_{1\alpha}$, that vanish when contracted with the external on-shell gluon polarizations $\epsilon_\alpha^a(p_1)$ and $\epsilon_\beta^b(p_2)$ respectively. It is easy to show that the required expression for $\bar{\Gamma}^{\alpha\beta\mu}$ is given by

$$\bar{\Gamma}^{\alpha\beta\mu} = \frac{2}{s}p_2^\alpha p_1^\beta\left(p_2^\mu - p_1^\mu\right) + 2\delta^{\mu\alpha}p_1^\beta - 2\delta^{\mu\beta}p_2^\alpha, \quad (15)$$

where, in Eq. (15), the indices α and β are understood to be contracted with the on-shell gluon polarization vectors $\epsilon_\alpha^a(p_1)$ and $\epsilon_\beta^b(p_2)$ respectively, with p_1 and p_2 momenta entering the 3-gluon vertex. When this new diagram $\bar{M}_s^A$ is added to the total amplitude M in Eq. (13) the effective amplitude $M_{GI} = M + \bar{M}_s^A$ turns out to be manifestly gauge invariant under the transformations $\epsilon_\mu^a(p_1) \to p_{1\mu}$ and $\epsilon_\mu^b(p_2) \to p_{2\mu}$ due to the relation (14). Finally, after a bit of algebra, one can prove that the following relation holds

$$\sum_{\rm pol}|M|^2 = \sum_{\rm pol}|M_{GI}|^2, \quad (16)$$

showing that the result for the cross-section in Eqs. (11),(12), including the term in M_{ss} proportional to $|g_A|^2$, is truly $SU(3)_c$ gauge invariant.

After integrating Eq. (11) over the full range of $\hat{t}$, we obtain for the total partonic cross section

$$\hat{\sigma}^{gg}(\hat{s}) = \frac{\pi\alpha_S^2}{48\hat{s}}\Big\{ (16+\rho\,(16+\rho))\log\left(\frac{1+\beta}{1-\beta}\right) - \beta\left(28+31\rho+6|g_A|^2\,(\rho-1)\right)\Big\}. \quad (17)$$

Our results for the cross sections appearing in Eqs.(8), (10), and (11), (12) are consistent with the corresponding QCD results [35] in the limit of $g_A^{q,t} \to 0$. Moreover, Eqs.(8), (10) are consistent with the corresponding results in the axigluon models [19], in the limit of vanishing axigluon mass and for the part concerning the vector-axial couplings.

Finally, the hadronic cross section $pp \to t\bar{t}X$ at LHC is obtained by convoluting the partonic cross sections in Eqs. (10),(17) with the corresponding parton distribution functions (PDF) for quarks and gluons, namely

$$\sigma_{pp\to t\bar{t}X} = \int\left(\sum_q d\mu_q\sigma_{qq}(\hat{s}) + d\mu_g\sigma_{gg}(\hat{s})\right), \quad (18)$$

where $d\mu_q$ and $d\mu_g$ indicate the differential integrations in dx_1dx_2 convoluted with the quarks and gluon PDF, respectively. In the numerical integration of Eq. (18) we have used the CTEQ6L1 parton distribution function (PDF) [36], where we set the PDF scale $\mu = m_t$ with top-quark mass $m_t = 172$ GeV.

IV. CHARGE ASYMMETRIES AT THE LHC

A. Definitions

Here we present the numerical results for the gluon axial-vector contribution to the $t\bar{t}$ charge asymmetry at the LHC. Let us first review the SM contribution to charge asymmetry.

In the SM, the angular and rapidity distributions of the top and anti-top quarks are identical at tree-level. However, a $t\bar{t}$ charge asymmetry (of order $\mathcal{O}(\alpha_S^3)$ can be generated at one-loop level by the interference of the tree-level diagram for the $q\bar{q} \to t\bar{t}$ process with the corresponding one-loop QCD box-contribution [16]. In particular, QCD predicts that top-quarks become more abundant in the direction of the incoming light quarks. The EW interactions, with the Z-boson exchange in the s-channel, does not contribute at the tree-level since the interference with the QCD s-channel diagram is vanishing because of the singlet color representation of the Z boson. At the Tevatron, the top-quark charge asymmetry is equivalent to the forward-backward (FB) asymmetry due to the charge conjugation symmetry of the initial $p\bar{p}$ state.

On the other hand, due to the symmetry of the colliding initial proton-proton state, the top-quark production at LHC is forward-backward symmetric in the laboratory frame. This means that, when integrated over the full kinematic range, the top-quark charge asymmetry vanish, as well as the the FB asymmetry. Nevertheless, it is still possible to get a non-vanishing charge asymmetry in suitable kinematic regions. The physical reason can be understood as follows. According to QCD, top-quarks are preferentially emitted in the direction of the incoming quarks. Since quarks have larger momenta than anti-quarks in the proton, the asymmetry at partonic level is transformed into an excess of top quarks in the forward and backwards regions due to the boost into the laboratory frame. This suggests that, when we restrict the sample of events to specific kinematic regions, a non-vanishing charge asymmetry can measured at the LHC.

Following the conventions adopted in Ref. [16], we are considering here the following set of charge asymmetries that can be measured at the LHC, defined as

- the **in** and **out** *cut-dependent* charge asymmetries

$$A_C^{\rm in}(y_C) = \frac{N(|y_{\bar{t}}| < y_C) - N(|y_t| < y_C)}{N(|y_{\bar{t}}| < y_C) + N(|y_t| < y_C)}, \quad (19)$$

$$A_C^{\rm out}(y_C) = \frac{N(|y_{\bar{t}}| > y_C) - N(|y_t| > y_C)}{N(|y_{\bar{t}}| > y_C) + N(|y_t| > y_C)}, \quad (20)$$

  as a function of the cut y_c on the top y_t and anti-top $y_{\bar{t}}$ quarks rapidities;

- the *cut-independent* charge asymmetry, as measured by ATLAS and CMS,

$$A_C = \frac{N(\Delta_y > 0) - N(\Delta_y < 0)}{N(\Delta_y > 0) + N(\Delta_y < 0)}, \quad (21)$$

  where $\Delta_y \equiv |y_t| - |y_{\bar{t}}|$;

- the *cut-dependent pair* charge-asymmetry

$$A_C^{\rm cut}(Y_c) = \frac{N(y_t > y_{\bar{t}}) - N(y_t < y_{\bar{t}})}{N(y_t > y_{\bar{t}}) + N(y_t < y_{\bar{t}})}, \quad (22)$$

  as a function of the cut Y_c on mean rapidity, namely $(y_t + y_{\bar{t}})/2 > Y_c$.

All the above observables are defined in the laboratory frame. Due to the symmetry of the initial proton-proton configuration, both $A_C^{\rm in/out}(y_C)$ and $A_C^{\rm cut}(Y_c)$ vanish if the whole rapidity spectrum is integrated, that is when y_c and Y_c approach their maximum kinematic allowed values.

The top-quark production by the gluon-gluon fusion mechanism, which is dominant at the LHC (namely 70% and 90% at 7 TeV and 14 TeV c.o.m. energy respectively), is charge symmetric under higher order corrections. Moreover, as can be seen from Eqs. (11)-(12), this mechanism remains charge symmetric also in the

presence of an effective axial-vector coupling contribution. Therefore, the charge antisymmetric contributions to top quark production are thus screened at the LHC mainly due to the gluon-gluon fusion. However, the contributions of the gluon-gluon collisions can be reduced by imposing a lower cut on the top-pair invariant mass m_{tt}. This has the effect of eliminating the regions of lower longitudinal momentum fraction of the colliding partons where the gluon density is much larger that the quark densities.

By imposing lower cuts on m_{tt} has also the advantage of enhancing the $q\bar{q} \to t\bar{t}$ contribution to the charge asymmetry, although at the price of reducing the statistics of $t\bar{t}$ pairs. As we will show in the following, this requirement has also crucial implications for our scenario, since it increases the contribution of the axial-vector coupling of gluon to the charge asymmetry. This is due to the fact that the effective coupling g_A grows as m_{tt}^2/Λ^2 at large m_{tt} values, but still $m_{tt} \leq \Lambda$.

Following the results of [24], we will restrict our analysis to the case of real and universal axial-vector gluon couplings. In particular, by neglecting higher order terms in q^2, we parametrize at low energy the axial-vector coupling (for values of $|q^2| < \Lambda^2$) as follows

$$g_A^t = g_A^q = \frac{q^2}{\Lambda^2} \,, \tag{23}$$

which corresponds to neglect the q^2 dependence in the form factor $F(q^2, M)$ in Eq.(3) and normalize it to 1. All NP couplings are then absorbed in the scale Λ.

Indeed, in order to explain the Tevatron anomaly on top-quark FB asymmetry, while requiring conservative constraints on the $t\bar{t}$ cross sections at Tevatron, in [24] it was suggested that the most favored scenario is the one where all axial-vector couplings are universal and real, with the NP scale Λ that lies in a narrow range 1 TeV $< \Lambda <$ 1.3 TeV.

However, we stress that the role of new free parameters proportional to the imaginary part of the axial-vector form factors, should not dramatically affect our results. The reason is the following. The charge asymmetry is directly proportional to the real part of the g_A form factors, in particular to $\mathrm{Re}[g_A^q]\mathrm{Re}[g_A^q]$, cfr. the last term in the right hand side (r.h.s.) of Eq. (8). On the other hand, the $\mathrm{Im}[g_A]$ enters only through $|g_A|$ in the denominators of Eqs. (19)-(22), thus it affects only the total cross section or analogously the total number of events in the asymmetry. Moreover, the NP contribution to the total $t\bar{t}$ cross section at LHC is largely screened by the QCD gluon-gluon production mechanism. Therefore, by requiring conservative constraints on the total cross section, the dependence of the charge-asymmetry by $\mathrm{Im}[g_A]$ will be strongly limited, justifying in part the fact that $\mathrm{Im}[g_A]$ does not play a crucial role in the present analysis.

In our numerical analysis we have not included the SM contribution to the charge asymmetry. Indeed, this is almost negligible with respect to the axial-vector gluon contribution for most of the kinematic regions considered here. In particular, we have retained only the g_A contribution in the numerators of the r.h.s. of Eqs. (19)-(22), neglecting the corresponding SM contribution. Clearly, we have retained the SM effect, at the leading order (LO) in QCD, in the evaluation of the total number of events entering in the equation for the charge asymmetry.

Following the definition of asymmetry, the full value of $A_C^{\mathrm{SM+NP}}$, including the SM one (A_C^{SM}), can be related to the results of A_C^{NP} presented here by the following relation

$$A_C^{\mathrm{SM+NP}} = A_C^{NP} + \frac{A_C^{\mathrm{SM}}}{1+\Delta\sigma} \,, \tag{24}$$

where, $\Delta\sigma$ is the percentage variation of the total cross section (defined as $\Delta\sigma = \sigma^{\mathrm{NP}}/\sigma^{SM}$), and $\sigma^{\mathrm{NP\ (SM)}}$ represent the pure NP (SM) contributions to the total cross sections evaluated in the same kinematic region of charge asymmetry. The numerical values of $\Delta\sigma$, as function of Λ and for some kinematic regions of m_{tt}, are plotted in Fig. 9. The symbol A_C appearing in the figures stands for the pure NP contribution to the charge asymmetry A_C^{NP} as defined above.

B. Numerical results

Our numerical results for the g_A contributions to the charge asymmetries, defined in Eqs. (19)-(22), together with their corresponding statistical significances, are shown in Figs. 4-8.

Regarding the statistical significance $S[A_C]$ for a generic charge asymmetry definition, we have used the approximated relation [19]

$$S[A_C] \simeq A_C \sqrt{L\,\sigma^{\mathrm{NP+SM}}} \,, \tag{25}$$

where L stands for the integrated luminosity and $\sigma^{\mathrm{NP+SM}}$ is the total cross section including SM and NP contribution. In $\sigma^{\mathrm{NP+SM}}$ we have used the LO cross sections multiplied by the rescaling factor K. This K factor is obtained by simply rescaling the total cross sections evaluated at the LO in QCD to its value corrected at the next-to-next-to-leading order (NNLO) in QCD [10, 11]. Although the difference is of order of few percent, we have used two separate rescaling factors for the LHC center of mass energies corresponding $\sqrt{S} = 7$ TeV and $\sqrt{S} = 14$ TeV. Moreover, we have assumed a universal K factor for different kinematic regions. All plots of significances, correspond to an integrated luminosity of $L = 10$ fb^{-1}. Notice that the significance in Eq.(25) is a simple theoretical estimation of the true one, since it does not take into account efficiencies, acceptance, resolution, and systematics.

In the left side plots of Fig. 4 we show the values of the **in** cut-dependent charge asymmetry A_C^{in}, as a function of the rapidity cut y_c in the range $0.1 < y_c < 3$, for four different kinematic regions [a-d], corresponding to m_{tt}

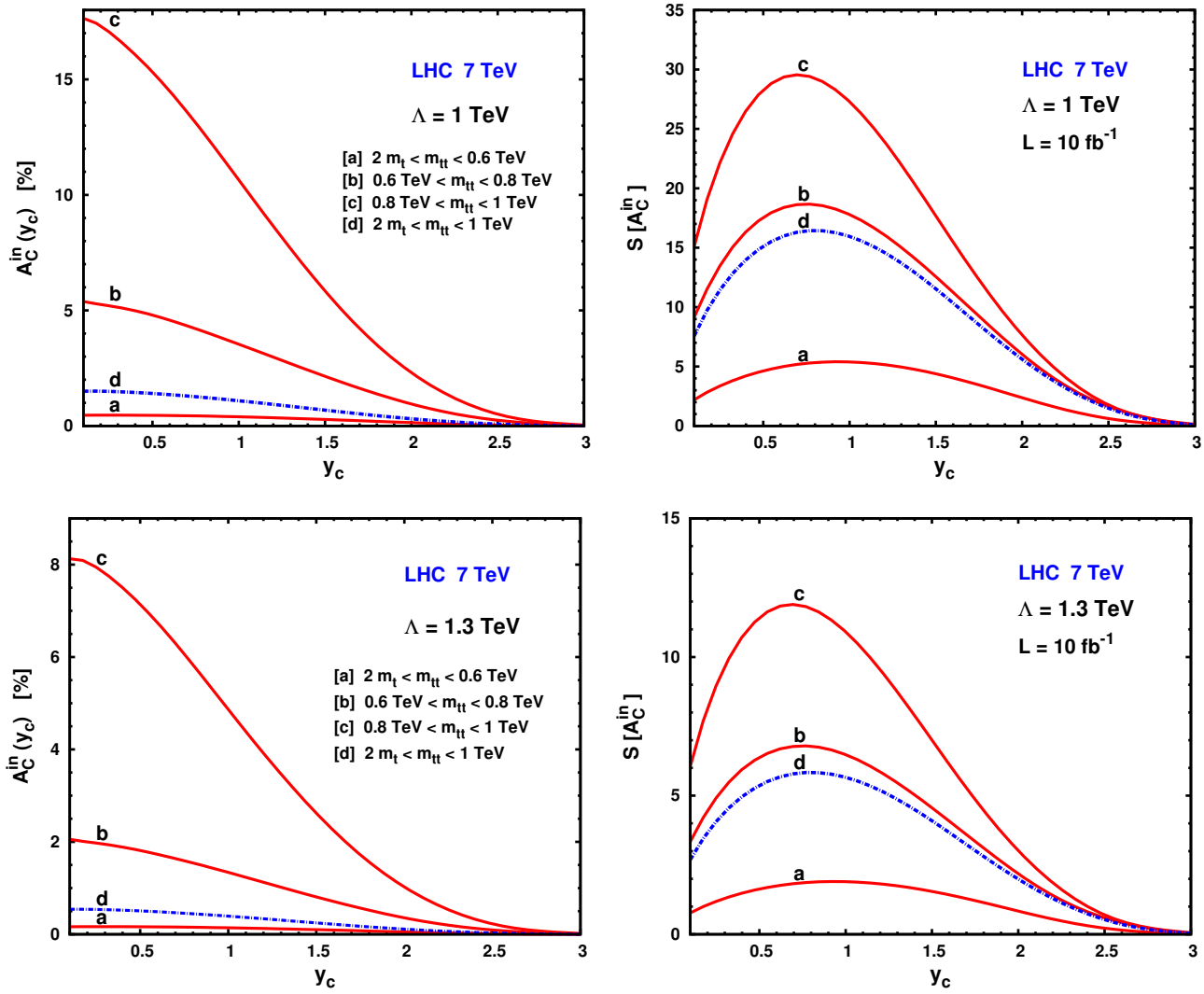

FIG. 4: The $t\bar{t}$ charge asymmetry $A_C^{in}(y_c)$ in percentage (left plots) and corresponding statistical significance $S[A_C^{in}]$ (right plots) at LHC with pp center of mass energy $\sqrt{S} = 7$ TeV and integrated luminosity $L = 10$ fb^{-1}, with $m_t = 172$ GeV, as a function of the cuts on the t- and $\bar{t}$-quark rapidity y_c (in the lab frame) and for several regions ([a-d]) of $t\bar{t}$ invariant mass m_{tt}. Up and down plots correspond to the scale $\Lambda = 1$ TeV and $\Lambda = 1.3$ TeV, respectively.

cuts in the following ranges:

$$\begin{aligned} [a] &= 2m_t < m_{tt} < 0.6 \text{ TeV}, \\ [b] &= 0.6 \text{ TeV} < m_{tt} < 0.8 \text{ TeV}, \\ [c] &= 0.8 \text{ TeV} < m_{tt} < 1 \text{ TeV}, \\ [d] &= 2m_t < m_{tt} < 1 \text{ TeV}, \end{aligned} \tag{26}$$

and for $\Lambda = 1$ TeV (top left-plot) and $\Lambda = 1.3$ TeV (down left-plot). We have used the same definition of m_{tt} ranges in Eq. (26) in all Figs. 4-7. From now on, if not specified, we will refer to the definition of [a]-[d] m_{tt} ranges according to Eq. (26).

The SM contribution to the top-quark charge asymmetries has been recently updated in Refs. [16, 17], where the one-loop EW corrections have been included, amounting roughly to 1.1% [16]. The SM predicts always a positive sign for all the charge asymmetries defined in Eqs. (19)-(22).

One general prediction of our scenario is that the effective axial-vector gluon coupling contributes to all top-quark charge asymmetries with the same sign as the SM one. From the results of Ref. [16] we can see that the magnitude of the SM contribution to $A_C^{\rm in}(y_c)$ is quite small, being below 1% in the full range of y_c.[1] On the other

[1] Notice that a direct comparison between our results and the SM predictions in [16] is actually misleading, since in [16] m_{tt} has been integrated over all the allowed kinematic range. In our scenario, this is not possible, being the low energy approximation for the g_A form factor only valid for values of $m_{tt} < \Lambda$. Nevertheless, due to the fact that the SM charge-asymmetry is weakly

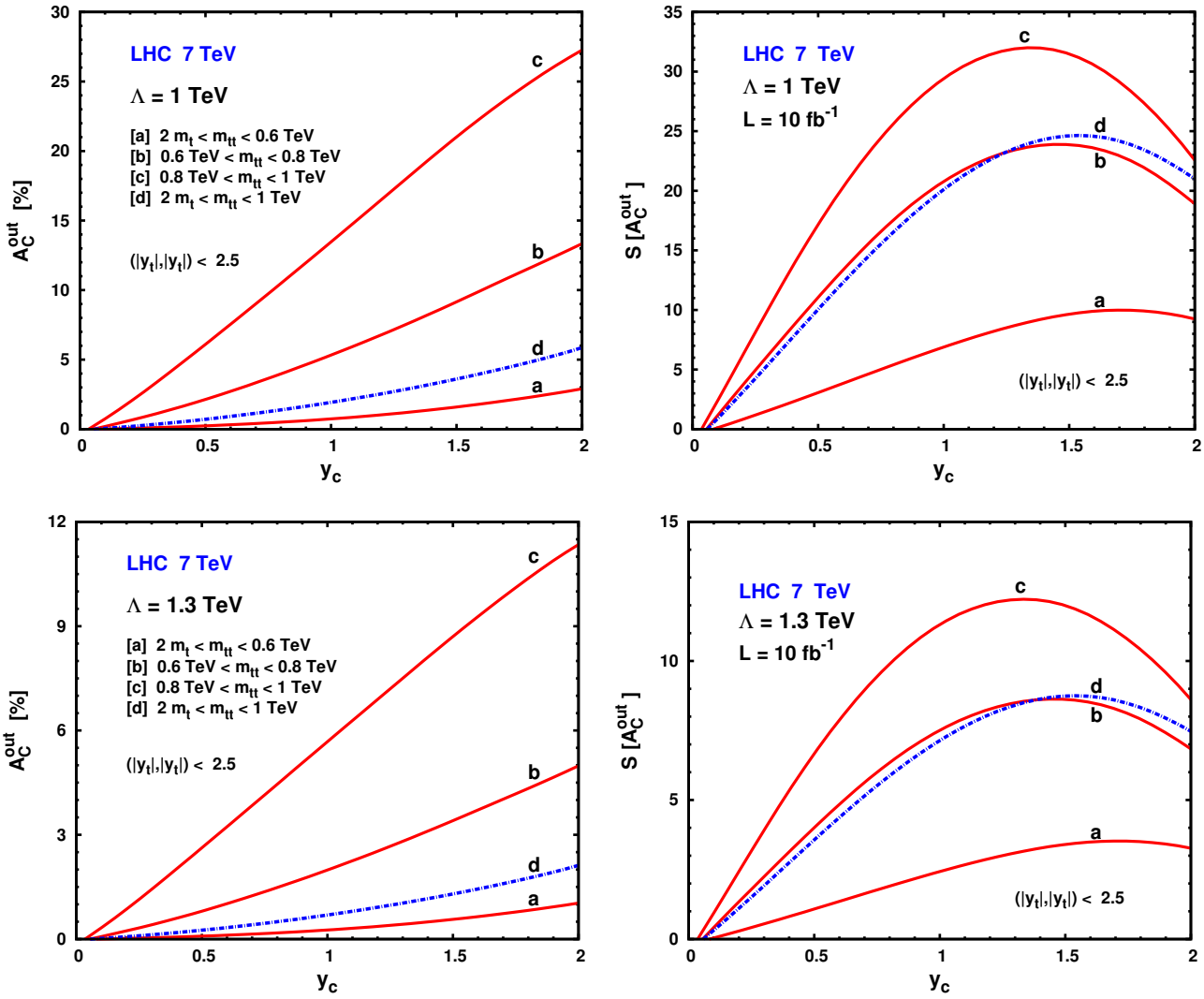

FIG. 5: The $t\bar{t}$ charge asymmetry $A_C^{out}(y_c)$ in percentage (left plots) and corresponding statistical significance $S[A_C^{out}]$ (right plots) at LHC with pp center of mass energy $\sqrt{S} = 7$ TeV and integrated luminosity $L = 10$ fb^{-1}, with $m_t = 172$ GeV, as a function of the cuts on the t- and $\bar{t}$-quark rapidity y_c (in the lab frame), for several regions ([a-d]) of $t\bar{t}$ invariant mass m_{tt}. The upper constraints on rapidities $(|y_t|, |y_{\bar{t}}|) < 2.5$ is imposed. Up and down plots correspond to the scale $\Lambda = 1$ TeV and $\Lambda = 1.3$ TeV, respectively.

hand, in our scenario $A_C^{\rm in}(y_c)$ can be substantially enhanced well above the few percent level, depending on the m_{tt} integrated regions.

In the right plots of Fig. 4, we show the values for the corresponding significance $S[A_C^{\rm in}]|$ as a function of y_c in the case of $\Lambda = 1$ TeV (up plot) and $\Lambda = 1.3$ TeV (down plot). From these results we can see that its maximum value is reached for rapidity cuts around $y_c \sim 0.7$, roughly in all m_{tt} ranges [a]-[d]. In particular, at $y_c = 0.7$ and for $L = 10$ fb^{-1}, we get $S[A_C^{\rm in}]|_{\rm max} \simeq (30, 19, 16, 6)$ for $\Lambda = 1$ TeV and $S[A_C^{\rm in}]|_{\rm max} \simeq (12, 7, 6, 2)$ for $\Lambda = 1.3$ TeV, corresponding to m_{tt}=([c],[b],[d],[a]), respectively. For these ranges, the values of the charge asymmetries in percentage are $A_C^{\rm in}[\%] = (14, 4.4, 1.3, 0.5)$ and $A_C^{\rm in}[\%] = (6.4, 1.6, 0.5, 0.2)$ for $\Lambda = 1$ TeV and $\Lambda = 1.3$ TeV, respectively.

In Fig. 5 we report the results for the $A_C^{\rm out}(y_c)$ asymmetry (left plots) and corresponding significance (right plots), as a function of the rapidity cuts y_c, obtained by also imposing an upper limit on top and anti-top rapidities, namely $|y_t| < 2.5$, $|y_{\bar{t}}| < 2.5$. According to these results, we can see that the maximum significance is reached in the range $y_c = [1.4 - 1.6]$,

dependent on m_{tt}, we expect that results in Ref. [16] will not dramatically change if restricted, for instance, to the kinematic region of $2m_t < m_{tt} < 1$TeV, where a direct comparison with our results is possible.

with $S[A_C^{\rm in}]|_{\rm max} \simeq (33, 24, 25, 10)$ for $\Lambda = 1$ TeV and $S[A_C^{\rm in}]|_{\rm max} \simeq (12, 9, 9, 3)$ for $\Lambda = 1.3$ TeV, corresponding to the m_{tt} ranges ([c],[b],[d],[a]), respectively. For the corresponding charge asymmetry in percentage, evaluated for instance at $y_c = 1.5$, we get $A_C^{\rm out}[\%] = (21, 9, 3.6, 1.6)$ and $A_C^{\rm out}[\%] = (8.8, 3.4, 1.3, 0.6)$ in the ranges ([c],[b],[d],[a]), for $\Lambda = 1$ TeV and $\Lambda = 1.3$ TeV, respectively. From these results we can see that $A_C^{\rm out}$ is more sensitive than $A_C^{\rm in}$ to the axial-vector coupling and at $y_c = 1.5$ can provide a larger asymmetry with better significance with respect to $A_C^{\rm in}$.

In Fig. 6 we plot the cut-independent $t\bar{t}$ charge asymmetry A_C (left plot) and corresponding significance (right plot) as a function of the scale Λ in the range [1-1.3] TeV. This is the definition adopted by the ATLAS [25] and CMS [26, 37] collaborations to measure the top-quark charge asymmetry at LHC. As shown from these results, the g_A contribution to A_C is quite large when measured at high m_{tt} masses close to the value of the scale Λ. In particular, for the range [c], A_C could be of order of 15% and 7%, for a scale $\Lambda = 1$ TeV and $\Lambda = 1.3$ TeV respectively, while its corresponding significance can reach values of 37 and 15, respectively. On the other hand, when integrated over a large m_{tt} range, see for instance the curve relative to [b] range, A_C turns out to be quite small (below 2 %) and comparable (although a bit larger) to the SM result [16].

Finally, in Fig. 7 we show the cut-dependent pair charge asymmetry $A_C^{\rm cut}(Y_c)$ as defined in Eq. (22) (left plots) and corresponding significance (right plots), as a function of the cuts Y_c on the mean rapidity $Y = (y_t + y_{\bar{t}})/2$, for the representative values of $\Lambda = 1, 1.3$ TeV. As we can see from these results, $A_C^{\rm cut}(Y_c)$ turns out to be the best sensitive probe of our scenario. In particular, at $\Lambda = 1$ TeV, for m_{tt} in the range [c], the value of $A_C^{\rm cut}(Y_c)$ can vary, as a function of Y_c, from 15% up to 55% for $\Lambda = 1$ TeV and from 7% up to 29% for for $\Lambda = 1.3$ TeV. The value of $A_C^{\rm cut}(Y_c)$ in the range [c] evaluated for $Y_c = 0.3$, where its significance is maximized, is of order of 20% and 10% for $\Lambda = 1$ TeV and $\Lambda = 1.3$ TeV, respectively. However, even at $Y_c = 1.5$ the cut-dependent pair charge asymmetry is still quite large. For $\Lambda = 1$ TeV, $A_C^{\rm cut}(1.5)$ is still of order 50% and 20% if integrated in the ranges [c] and [b] respectively, while the corresponding significances are still above 10. However, for $\Lambda = 1.3$ TeV, the value of $A_C^{\rm cut}(1.5)$ drops down to 25% and 7% for m_{tt} ranges [c] and [b] respectively, with a corresponding significance of order 5.

In Fig. 8 we analyzed the statistical significance of the cut-independent charge asymmetry A_C versus the scale Λ in the range of Λ=[1.5-4] TeV and for several ranges of m_{tt} as indicated in the figure. In particular, the left and right plots correspond to the LHC center of mass energies of $\sqrt{S} = 7$ TeV and $\sqrt{S} = 14$ TeV, respectively. Regarding the choice of ranges of m_{tt}, we adopted the criteria that the maximum value of the m_{tt} satisfies the condition $m_{tt}^{\rm max} \leq \Lambda$ as required by the validity range of the low energy limit in the g_A form factor. Assuming that no sensitive deviations from SM predictions on the charge asymmetry A_C will be observed, from results in Fig. 8 one can derive lower bounds on the scale Λ. For example, by requiring that $S[A_C] < 3$, we get for $L = 10$ fb^{-1}, the following (strongest) lower bounds:

- $\Lambda > 2.6$ TeV, for $m_{tt} \in$ [1.5-2] TeV at LHC 7 TeV;
- $\Lambda > 3.7$ TeV, for $m_{tt} \in$ [2.5-3] TeV at LHC 14 TeV .

As can be seen from the dashed (blue) curves in the left plot of Fig. 8, for LHC 7 TeV there is not any advantage, concerning the lower bounds of Λ, in going to higher bin ranges in $m_{tt} > 2$ TeV, due to the loss of statistics.

In Fig. 9 we plot the percentage variation $\Delta\sigma$ of the total cross section for $pp \to t\bar{t}$ at LHC for LHC 7 TeV (left) and LHC 14 TeV (right), as a function of Λ from 1 TeV to 5 TeV, and for several ranges of m_{tt}. The $\Delta\sigma$ is defined after Eq. (24) and cross sections have been evaluated at the LO in QCD. The picture that emerges from these results is clear. If we analyze ranges of m_{tt} below 1 TeV scale, see the curve corresponding to the [a] range, the expected percentage variation in the total cross section is quite small, being below 5% in both energy ranges at LHC 7 TeV and 14 TeV. This is due to the fact that requiring m_{tt} to be below 1 TeV, the g_A contribution at low energy is still largely screened by the gluon-gluon fusion mechanism, which is the dominant mechanism of top-quark pair production at LHC. Clearly, by increasing the m_{tt} mass range the NP effect could be amplified and larger deviations could be observed in the cross sections, due to the quark-antiquark production mechanism. These results could also be used to set lower bounds on the scale Λ by requiring that no excess in the total cross section is observed with respect to the SM predictions. For instance, by limiting the deviations on total cross section below 20 %, one can see from the curve [e] that a lower bound $\Lambda > 4$ TeV could be obtained at LHC 7 TeV. Clearly, by increasing the m_{tt} range, the statistical error on the cross section also increases, and a more accurate analysis, which is going beyond the purpose of the present paper, would be necessary.

V. CONCLUSIONS

We studied the gluon effective axial-vector coupling induced top charge asymmetries at the LHC. We compared rapidity cut-dependent and independent asymmetries and showed that the former are more sensitive to NP than the latter. We also studied the asymmetries and variations of total $t\bar{t}$ cross sections at different invariant masses of the $t\bar{t}$ system and showed that it would be necessary to measure those quantities as functions of m_{tt} at the LHC. If this is done, 7 TeV LHC has enough sensitivity either to confirm the Tevatron top charge asymmetry anomaly or to rule it out in the context of considered NP scenario. In the latter case the LHC is able to put stringent constraint on the NP scale Λ.

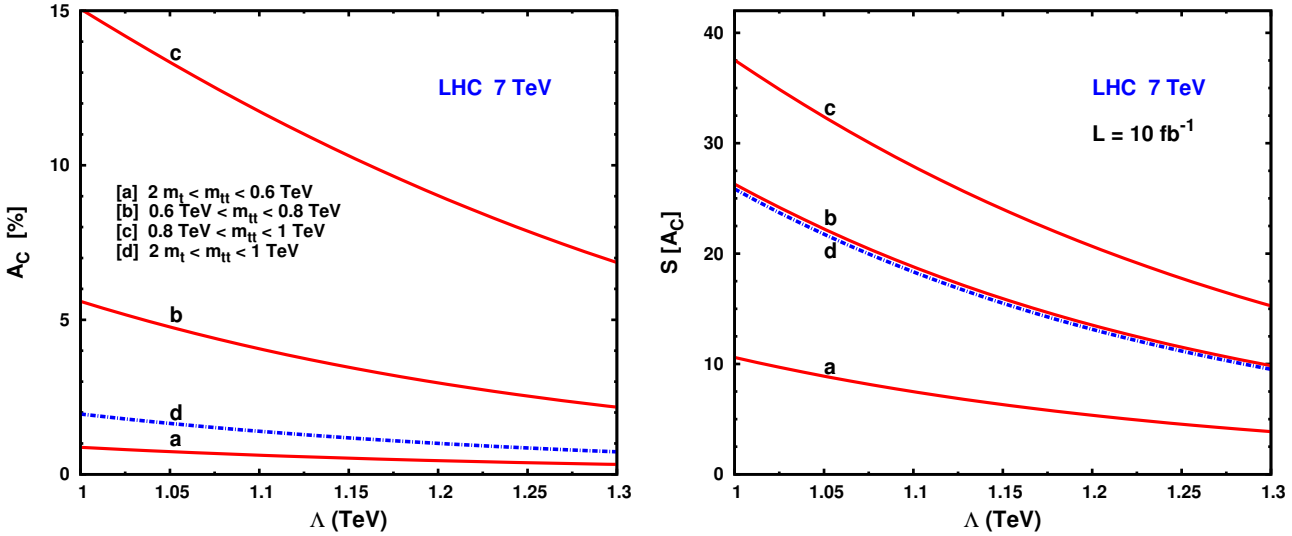

FIG. 6: The cut-independent $t\bar{t}$ charge asymmetry A_C in percentage (left plots) and corresponding statistical significance $S[A_C]$ (right plots) at LHC with pp center of mass energy $\sqrt{S} = 7$ TeV and integrated luminosity $L = 10$ fb^{-1}, with $m_t = 172$ GeV, as a function of the scale Λ in TeV, for several regions ([a-d]) of $t\bar{t}$ invariant mass m_{tt}.

Acknowledgment

We thank T. Chwalek, A. Giammanco, T. Peiffer, G. Rodrigo, and J. Wagner-Kuhr for several communications. This work was supported by the ESF grants 8090, MTT59, MTT60, JD164, by the recurrent financing SF0690030s09 project and by the European Union through the European Regional Development Fund.

[1] T. Aaltonen et al. (CDF Collaboration), Phys.Rev. **D83**, 112003 (2011), 1101.0034.
[2] V. M. Abazov et al. (D0 Collaboration) (2011), 1107.4995.
[3] J. H. Kuhn and G. Rodrigo, Phys.Rev.Lett. **81**, 49 (1998), hep-ph/9802268.
[4] J. H. Kuhn and G. Rodrigo, Phys.Rev. **D59**, 054017 (1999), hep-ph/9807420.
[5] M. Bowen, S. Ellis, and D. Rainwater, Phys.Rev. **D73**, 014008 (2006), hep-ph/0509267.
[6] O. Antunano, J. H. Kuhn, and G. Rodrigo, Phys.Rev. **D77**, 014003 (2008), 0709.1652.
[7] V. Ahrens, M. Neubert, B. D. Pecjak, A. Ferroglia, and L. L. Yang, Phys.Lett. **B703**, 135 (2011), 1105.5824.
[8] M. Cacciari, S. Frixione, M. L. Mangano, P. Nason, and G. Ridolfi, JHEP **0809**, 127 (2008), 0804.2800.
[9] S. Moch and P. Uwer, Phys.Rev. **D78**, 034003 (2008), 0804.1476.
[10] N. Kidonakis (2009), 0909.0037.
[11] N. Kidonakis (2011), 1105.3481.
[12] T. Aaltonen et al. (The CDF Collaboration), Phys.Rev. **D82**, 052002 (2010), 1002.2919.
[13] V. Abazov et al. (D0 Collaboration), Phys.Lett. **B679**, 177 (2009), 0901.2137.
[14] Tech. Rep. ATLAS-CONF-2011-140, CERN, Geneva (2011).
[15] Tech. Rep. CMS-PAS-TOP-11-007, CERN, Geneva (2011).
[16] J. H. Kuhn and G. Rodrigo (2011), 1109.6830.
[17] W. Hollik and D. Pagani, Phys.Rev. **D84**, 093003 (2011), 1107.2606.
[18] S. Westhoff (2011), 1108.3341.
[19] P. Ferrario and G. Rodrigo, Phys.Rev. **D78**, 094018 (2008), 0809.3354.
[20] P. Ferrario and G. Rodrigo, Phys.Rev. **D80**, 051701 (2009), 0906.5541.
[21] G. Rodrigo and P. Ferrario, Nuovo Cim. **C33**, 04 (2010), 1007.4328.
[22] S. Jung, H. Murayama, A. Pierce, and J. D. Wells, Phys.Rev. **D81**, 015004 (2010), 0907.4112.
[23] K. Cheung, W.-Y. Keung, and T.-C. Yuan, Phys.Lett. **B682**, 287 (2009), 0908.2589.
[24] E. Gabrielli and M. Raidal, Phys.Rev. **D84**, 054017 (2011), 1106.4553.
[25] Tech. Rep. ATLAS-CONF-2011-106, CERN, Geneva (2011).
[26] Tech. Rep. CMS-PAS-TOP-11-014, CERN, Geneva (2011).
[27] P. Haberl, O. Nachtmann, and A. Wilch, Phys.Rev. **D53**, 4875 (1996), hep-ph/9505409.
[28] Z. Hioki and K. Ohkuma, Eur.Phys.J. **C65**, 127 (2010), 0910.3049.
[29] K. Blum et al., Phys. Lett. **B702**, 364 (2011), 1102.3133.
[30] M. Raidal and A. Santamaria, Phys. Lett. **B421**, 250 (1998), hep-ph/9710389.
[31] C. Delaunay, O. Gedalia, Y. Hochberg, G. Perez, and Y. Soreq, JHEP **1108**, 031 (2011), 1103.2297.
[32] V. Khachatryan et al. (CMS Collaboration),

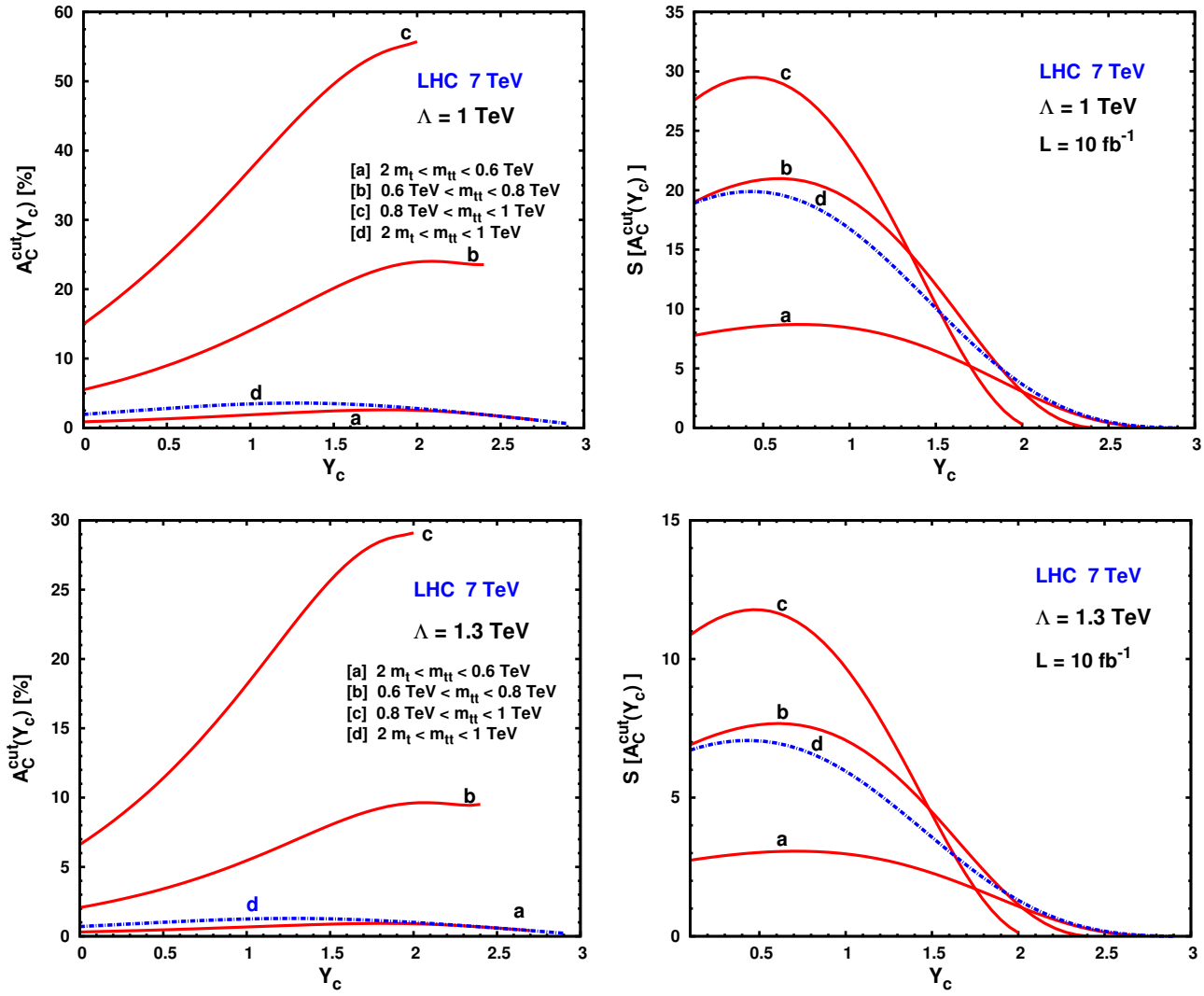

FIG. 7: Cut-dependent pair charge asymmetry $A_C^{\rm cut}(Y_c)$ in percentage (left plots) and corresponding statistical significance $S[A_C^{\rm cut}(Y_c)]$ (right plots) at LHC with pp center of mass energy $\sqrt{S} = 7$ TeV and integrated luminosity $L = 10$ fb^{-1}, with $m_t = 172$ GeV, as a function of the cuts on the mean rapidity $|Y| > Y_c$ (in the lab frame), for several regions ([a-d]) of $t\bar{t}$ invariant mass m_{tt}. Up and down plots correspond to the scale $\Lambda = 1$ TeV and $\Lambda = 1.3$ TeV, respectively.

Phys.Rev.Lett. **106**, 201804 (2011), 1102.2020.

[33] G. Aad et al. (ATLAS Collaboration), New J.Phys. **13**, 053044 (2011), 1103.3864.

[34] K. D. Lane (1996), hep-ph/9605257.

[35] W. Beenakker et al., Nucl. Phys. **B411**, 343 (1994).

[36] J. Pumplin, D. Stump, J. Huston, H. Lai, P. M. Nadolsky, et al., JHEP **0207**, 012 (2002), hep-ph/0201195.

[37] S. Chatrchyan et al. (CMS Collaboration) (2011), 1112.5100.

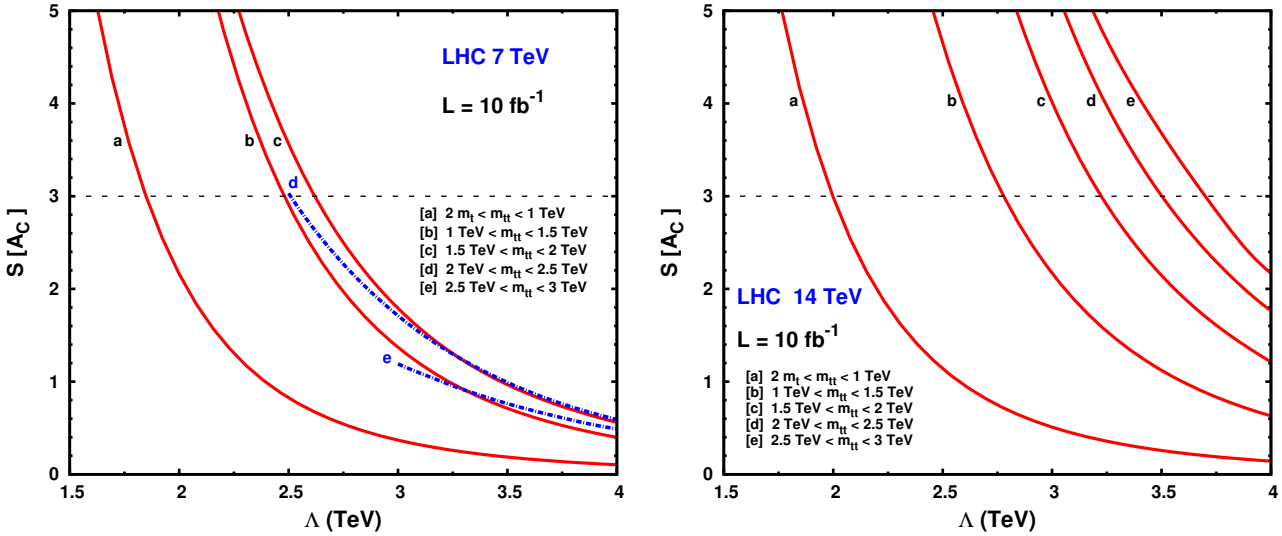

FIG. 8: Statistical significance $S[A_C]$ of the cut-independent $t\bar{t}$ charge asymmetry A_C at LHC with pp center of mass energies $\sqrt{S} = 7$ TeV (left plots) and $\sqrt{S} = 14$ TeV (right plot) with integrated luminosity $L = 10$ fb^{-1}, with $m_t = 172$ GeV, as a function of the scale Λ in TeV, for several regions ([a-e]) of $t\bar{t}$ invariant mass m_{tt}.

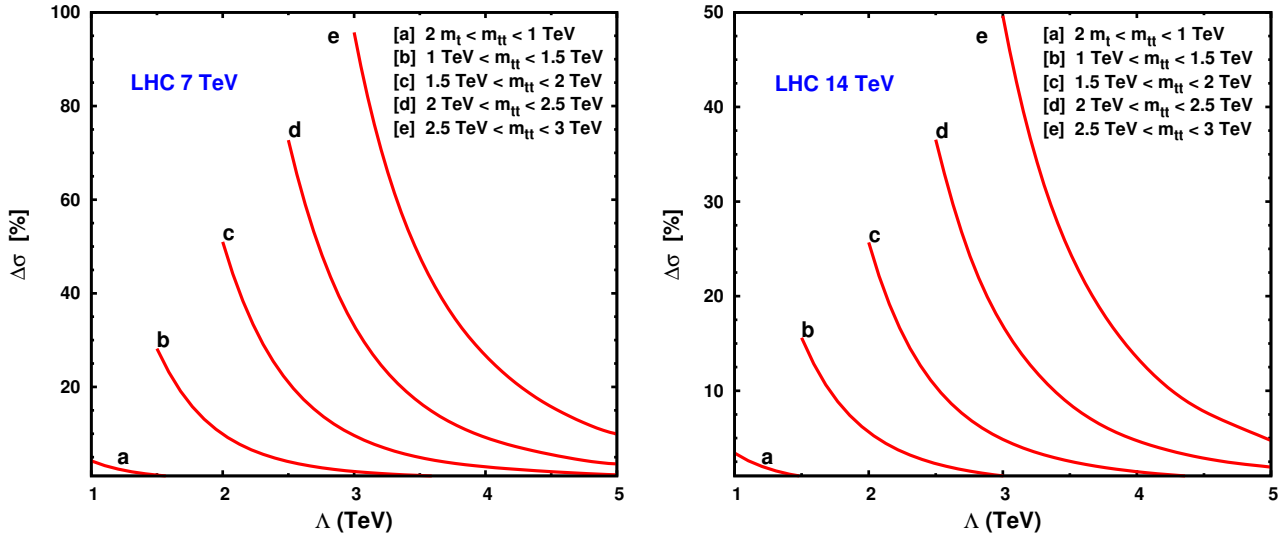

FIG. 9: Percentage variation $\Delta\sigma$ of the total cross section for $pp \to t\bar{t}$ at LHC with pp center of mass energies $\sqrt{S} = 7$ TeV (left plots) and $\sqrt{S} = 14$ TeV (right plot) for $m_t = 172$ GeV, as a function of the scale Λ in TeV, for several regions ([a-e]) of $t\bar{t}$ invariant mass m_{tt}.